

Experimental and analytical investigation of high-strength concrete-filled steel tube square columns subjected to flexural loading

Kyung-Soo Chung¹, Jin-Ho Kim¹ and Jung-Han Yoo^{*2}

¹Steel Structure Research Division, RIST, 180-1 Songdo-Dong,
Yeonsu-Gu, Incheon 406-840, Republic of Korea

²School of Architecture, Seoul National University of Science & Technology,
232 Gongreung-ro, Nowon-gu, Seoul, 139-743, Republic of Korea

(Received March 14, 2012, Revised December 26, 2012, Accepted January 19, 2013)

Abstract. The concrete-filled steel tube (CFT) columns have several benefits of high load-bearing capacity, inherent ductility and toughness because of the confinement effect of the steel tube on concrete and the restraining effect of the concrete on local buckling of steel tube. However, the experimental research into the behavior of square CFT columns consisting of high-strength steel and high-strength concrete is limited. Six full scale CFT specimens were tested under flexural moment. The CFT columns consisted of high-strength steel tubes ($f_y = 325$ MPa, 555 MPa, 900 MPa) and high-strength concrete ($f_{ck} = 80$ MPa and 120 MPa). The ultimate capacity of high strength square CFT columns was compared with AISC-LRFD design code. Also, this study was focused on investigating the effect of high-strength materials on the structural behavior and the mathematical models of the steel tube and concrete. Nonlinear fiber element analyses were conducted based on the material model considering the cyclic bending behavior of high-strength CFT members. The results obtained from the numerical analyses were compared with the experimental results. It was found that the numerical analysis results agree well with the experimental results.

Keywords: concrete-filled steel tube; high-strength steel; high-strength concrete; experimental research; nonlinear fiber element analysis

1. Introduction

A large section is required for normal-strength column members when both high-axial force and bending moment are applied in high-rise buildings. However, section reduction is an important issue in the structural system in terms of the serviceability performance of structures. To acquire the lease area based on section reduction and to maximize the efficiency of the floor plan area, high-strength steel and concrete were considered for a construction project.

The concrete-filled tube structure (CFT) member is an excellent composite member in terms of the structural, constructional, and fire-resistant aspects. Therefore, this study aimed to examine the structural characteristics of high-strength CFT members consisting of high-strength steel and

*Corresponding author, Assistant Professor, E-mail: happyjh@seoultech.ac.kr

concrete.

There have been many studies on high-strength CFT members. Uy and Mursi (2001a, 2001b, 2004) investigated axial and flexural test and analytical results with high strength steel tubes (750 MPa yield strength) and 20~32 MPa compressive strength concrete. Varma *et al.* (2002, 2004) proposed a structural-performance test and numerical analysis method for CFT beam-column members consisting of 110 MPa concrete and 269~660 MPa steel tubes. Liu and Gho (2003, 2005) estimated the axial behavior by conducting a compressive test of CFT columns made with 55~105 MPa-compressive-strength concrete and steel tubes with 300, 495, and 550 MPa yield strength, while comparing them to the current design code. Fujimoto *et al.* (2004) performed experimental studies on CFT members subjected to eccentric loading consisting of concrete with 25~80 MPa compressive strengths, and steel tubes with 262~834 MPa yield strength. They also proposed analytical models considering local buckling and confinement effect of steel tube, and made a comparison between experiments and analyses. Mursi and Uy (2006a, 2006b) conducted the analytical and experimental investigation of the behavior of hollow and CFT columns with high strength steel tubes (690 MPa yield strength) under biaxial loading. They also made a comparison between the test results and the results obtained from the existing codes and suggested a design approach. Choi *et al.* (2008) proposed the P-M interaction diagram of CFT members with 50~110 MPa compressive-strength concrete and steel tubes with 262~834 MPa yield strength. Han *et al.* (2003) tested and established a mechanical model for the CFTs using conventional strength materials with compressive strength f_{ck} between 20 and 60 MPa and yield stress f_y between 300 and 340 MPa. However, only few studies have focused on the structural performance of CFT members with high-strength materials or those with over 80 MPa-compressive strength concrete and over 650 MPa yield strength steel tubes.

Therefore, this study aimed at estimating the structural behavior of high-strength square CFT columns. Firstly, flexural tests of CFT were conducted with 80 MPa and 120 MPa concrete compressive strengths and of SM490, HSB600, and HSA800 steel (800 MPa class high tensile strength steel plate for buildings). Secondly, a nonlinear fiber element analysis method was proposed. To verify the proposed fiber element analysis method, the result of the fiber element analyses and the test results were compared.

2. Flexural tests

Table 1 Welding conditions for specimens

Welding condition	Type of steel		
	SM490	HSB600	HSA800
Welding method	FCAW	FCAW	FCAW
Welding rod	E71T-1	E81T-Ni1	E115T5-K4M
Shielding flux gas	CO ₂	CO ₂	CO ₂ (20%)+ Ar(80%)
Heat/temperature between passes (C)	10-250	75-250	75-250
Welding current (A)	380-400	280-300	260-280
Welding speed (cm/min)	30-45	30-45	30-45
Heat treatment after welding (C/hr)	590-650	590-650	590-650

2.1 Flexural specimens and parameters

Fig. 1 shows the details and dimensioned of the tested high strength CFT members. The specimen was a boxed sectional member made with 4-seam welded 20 mm thick steel plates. The top and bottom of the specimen were welded at the end plate to connect to the loading block. Welding conditions for specimens based on types of steels are shown in Table 1. The dimensions were \square -400 × 400 × 20 mm³, and the testing length (L) for specimen was 960 mm as shown in Fig. 1. A 100-mm-diameter hole was chosen so that concrete fill, with 13mm aggregate, could be placed and adequately compacted using external vibrator, when the specimens were standing vertically. And a 26-mm-diameter air hole was installed for checking of concrete compactness by examining the concrete released through the air hole.

All specimens were cast from the same batch of concrete and cured by covering it with a vinyl cap until the time of testing. The test specimens were listed in Table 2 to investigate bending behaviour of CFT by using high strength steel tubes and concrete. Variables parameters were concrete compressive strength (80 MPa and 120 MPa) and steel yield strength (325 MPa, 555 MPa and 900 MPa).

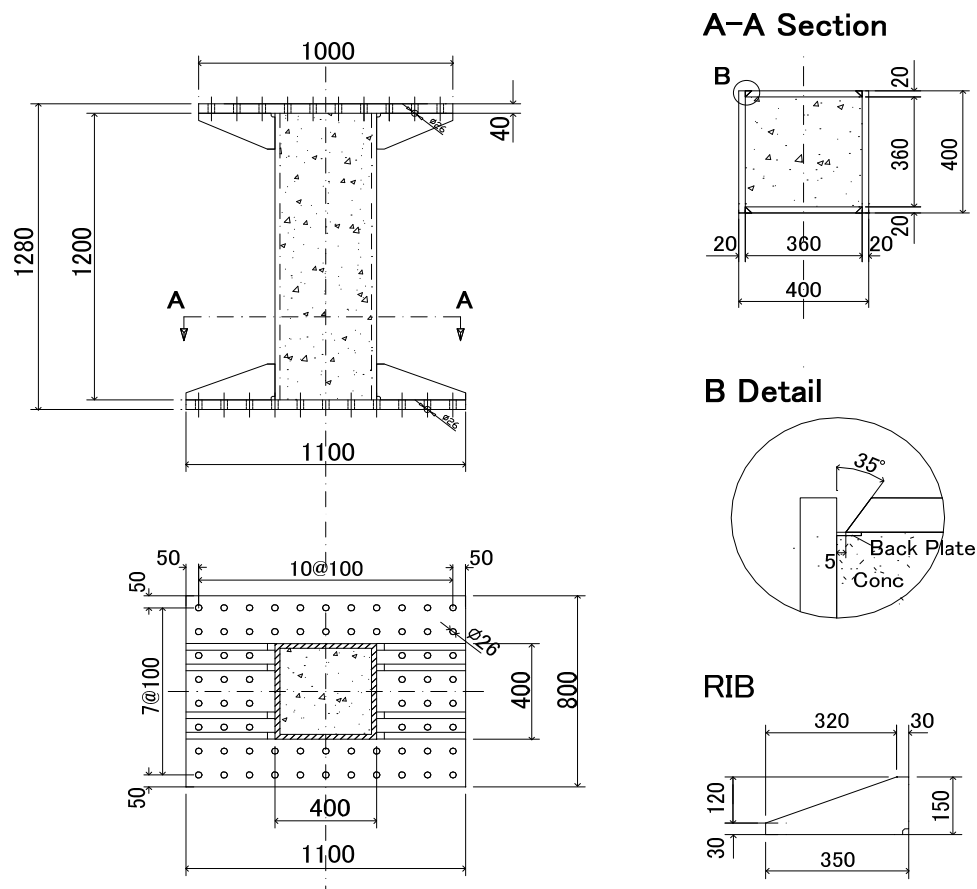


Fig. 1 Specimen and details

The basic material properties observed for each CFT steel tube are listed in Table 3. The values of the material properties are the average of three steel coupon tensile tests. The dimensions of all the tension coupons are illustrated in Fig. 2. In the conducted test for HSB600 and HSA800, there was no apparent yield plateau in the stress-strain relations of steel plates. The yield stress was determined as stress corresponding to offset strain 0.2%. The maximum failure load, yield strains and yield stress in tension can be obtained from the test results by plotting the stress-strain diagram as shown in Fig. 3. The concrete mix was designed to achieve specified 28 day strength of 80 MPa and 120 MPa, a maximum aggregate size of 13 mm and 600 mm slump flow.

The concrete cylinders were tested at 3, 7, and 28 days after casting so that strengths were available at the time the flexural tests were done. The average concrete compressive strength can be obtained from Table 4. The average cube strength of the concrete was 82.5 MPa and 119.7 MPa for specimens at the time of the flexural test. The concrete material properties were determined by conducting uni-axial compression tests on three concrete cylinders ($\Phi 100 \times 200 \text{ mm}^2$).

Table 2 Specimens

Specimen	Parameter	
	Yield Strength of Steel Tube (MPa)	Compressive Strength of Concrete (MPa)
C_490_80	325 (SM490)	82.5
C_490_120		119.7
C_600_80	555 (HSB600)	82.5
C_600_120		119.7
C_800_80	901 (HSA800)	82.5
C_800_120		119.7

Table 3 Mechanical properties of steel

Steel	Yield stress (MPa)	Tensile strength (MPa)	Yield ratio	Elongation (%)
SM490	325	518	0.62	29
HSB600	555	669	0.83	19
HSA800	901	965	0.93	12

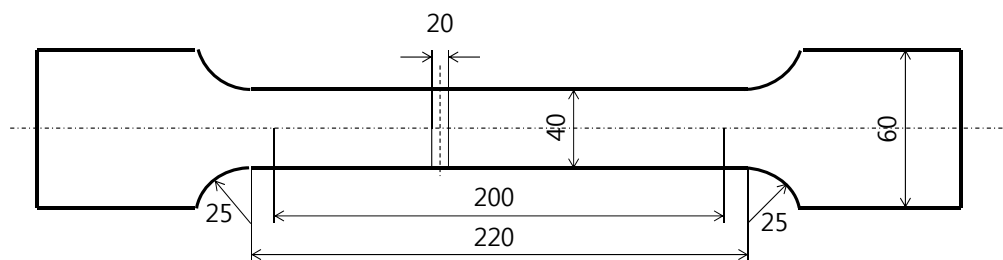


Fig. 2 Dimensions of a tensile coupon

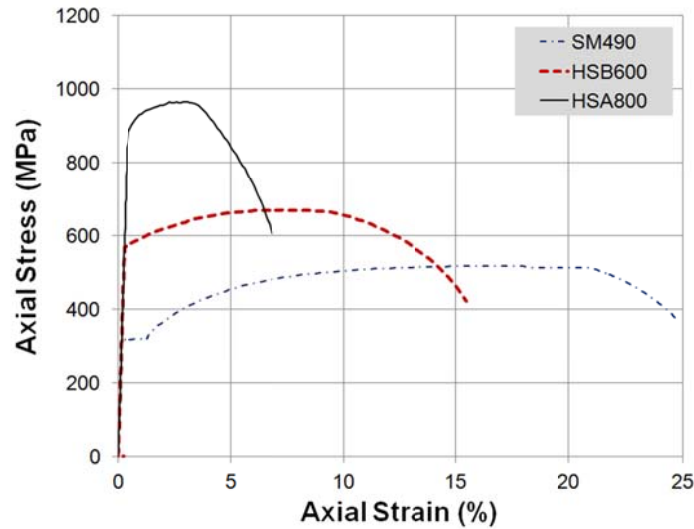


Fig. 3 Stress-strain curves

Table 4 Compressive strength test of concrete

Design compressive strength (MPa)	Compressive strength at elapsed days after pouring		
	3day	7day	28day
80	41.7	63.1	82.5
120	82.7	92.3	119.7

2.2 Test set-up

The test set-up for square CFT members subjected to bending moment is shown in Fig. 4(a). Applied loading was used 10 MN UTM which is displacement-controlled mechanical testing machine and three points bending method was used under shear and bending moment. The load was measured with load cells built-in tester. The loading rate of the cross head was 5.0 mm/min. The deformation of the specimen was measured with vertical displacements and rotation on central loading points and at both supports as shown in Fig. 4(b). This, in turn, measured the vertical displacement at supports, and the vertical displacement and rotation at the loading point.

To predict the occurrence of local buckling and the plasticity of the steel tube, two strain gauges were installed on the upper and lower flanges as shown in Fig. 4(c). This was about half the width of the member away from the loading points, and another three strain gages were installed on the left and right webs respectively.

Load is applied by the member rotation controlled loading protocol, as shown in Fig. 5. That is, loading history was one-direction incremental displacement amplitude loading. The member rotation is defined as the average value of the vertical displacements on the loading points divided by the member length. After applying maximum loads, the test was terminated when the load decreased to a point below each cycle's maximum load, when the rotation of the member reached 5%, or when welding failure occurred.

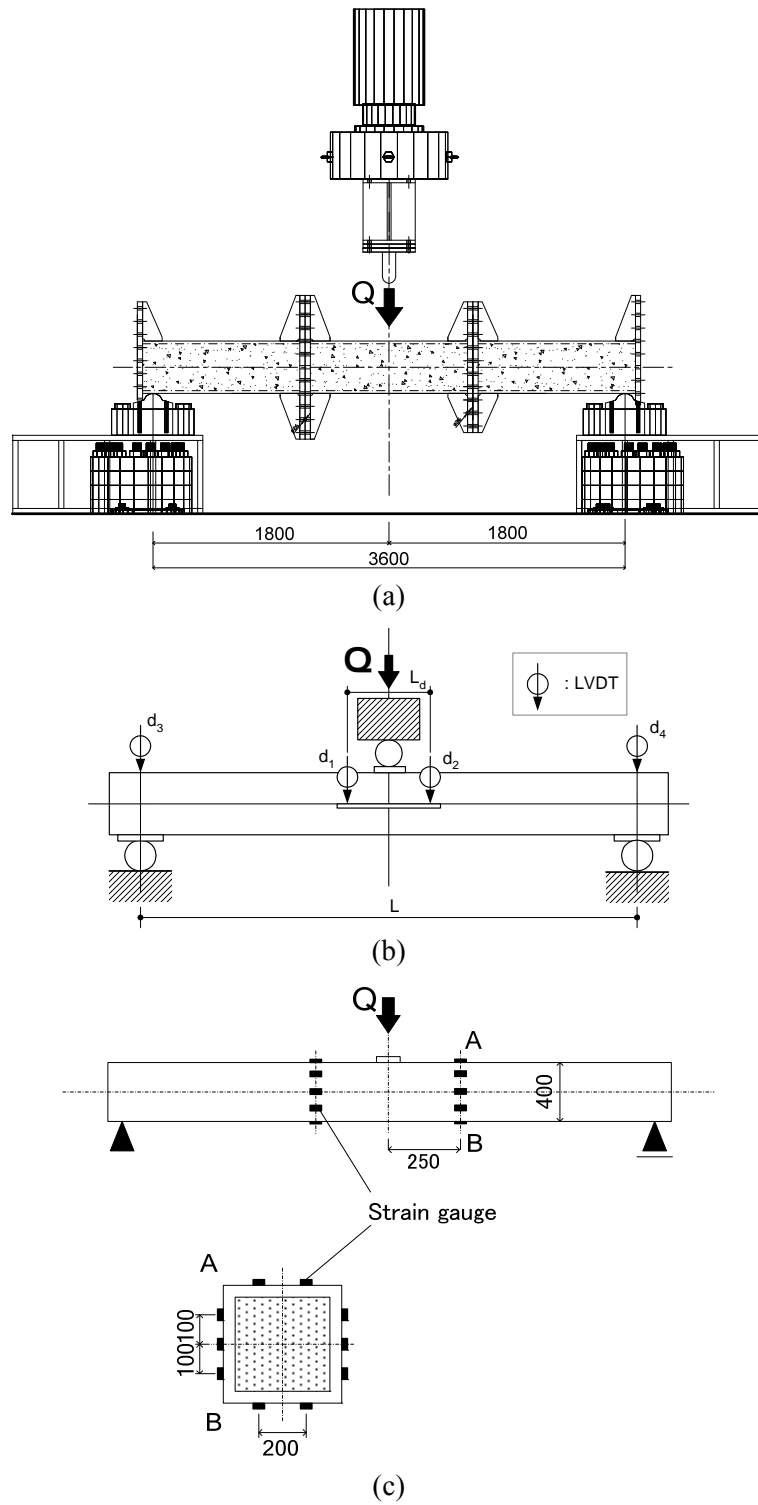


Fig. 4 Test set-up and locations of measurement: (a) Test set-up; (b) installation of displacement measurement; and (c) locations of strain gauges

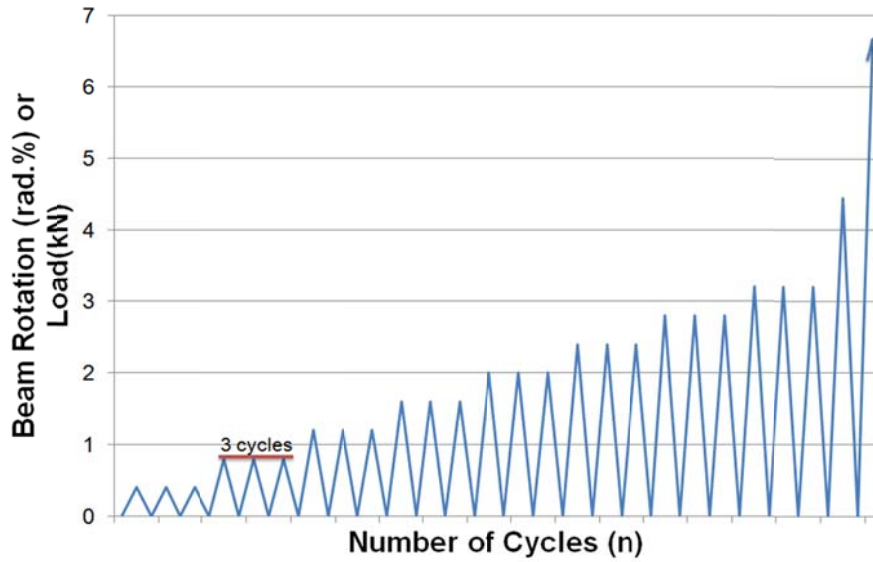


Fig. 5 Loading history

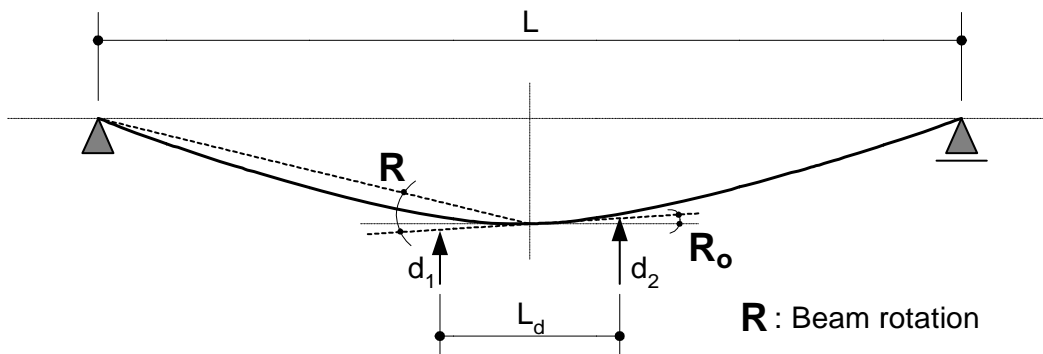


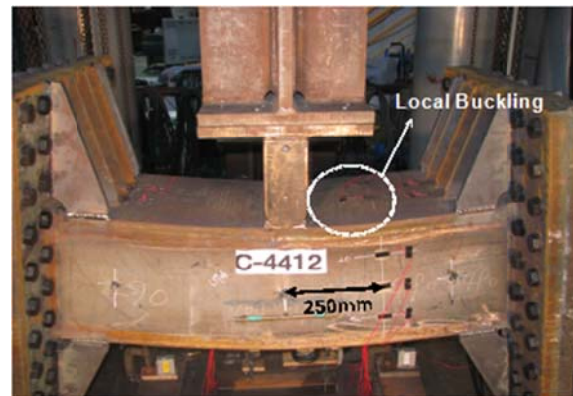
Fig. 6 Definition of member rotation

As shown in Fig. 6, Member (beam) rotation obtained from displacement measurement and member length was calculated based on Eq. (1)

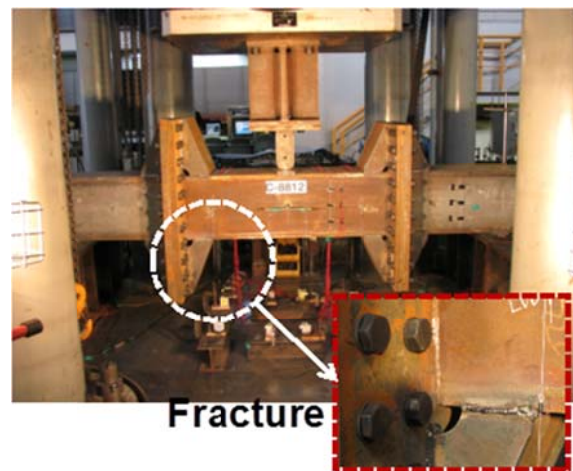
$$R = \frac{(d_1 + d_2) - (d_3 + d_4)}{L/2} + R_o \tag{1}$$

$$R_o = \frac{d_1 - d_2}{L_d} - \frac{d_3 - d_4}{L} \tag{2}$$

where, d_1, d_2, d_3, d_4 : vertical displacement of LVDT
 L_d : distance between d_1 and d_2
 L : member length (= 3600 mm)



(a) Local buckling



(b) Weld fracture

Fig. 7 Failure modes

2.3 Test results

2.3.1 Failure modes

Fig. 7 shows failure modes of the steel tubes after the tests. Failure occurred when an upward buckle of the top flange of the steel cross section at the distance of an approximately 150~200 mm from the loading point. A flange buckle is shown in Fig. 7(a).

The other was welding fracture of connection between endplate and steel tube after yielding of the HSA800 steel specimen. The welding fracture is because welding strength is lower than material strength. Therefore, the welding method on high strength steel is needed further research.

2.3.2 Moment-rotation relation

The moment-rotation curve is shown in Figs. 8 and 13. The initial stiffness is almost the same regardless of steel tube and concrete strength. After the maximum moment, the post-peak moment resistance decreases slowly without the effect of high strength concrete. This is because the width

to thickness (b/t) is small and the post-buckling for steel tube is resisted by filled concrete.

2.3.3 Initial stiffness

The initial stiffness of the specimens was shown in Table 5. The initial stiffness was calculated with the moment-rotation curve using the data at 10% and 50% of yield strength. There was minimal change in the initial stiffness regardless of the strength of steel tube and concrete.

The initial stiffness based on the AISC-LRFD code provisions (Leon and Hajjar 2008) can be predicted as follows

$$K_{ic} = \frac{6EI_{eff}}{L} \quad (3)$$

$$EI_{eff} = E_s I_s + C_1 E_c I_c \quad (4)$$

$$C_1 = \left(0.6 + 2 \left(\frac{A_s}{A_c + A_s} \right) \right) \leq 0.9 \quad (5)$$

$$E_c = 0.043 \times 2300^{1.5} \times \sqrt{f_{ck}} \quad (6)$$

where, E_s : young modulus in steel tube (= 200,000 MPa)
 EI_{eff} : effective flexural stiffness in composite member
 L : member length (= 3600 mm)
 f_{ck} : compressive strength on concrete (82.5 MPa and 119.7 MPa)

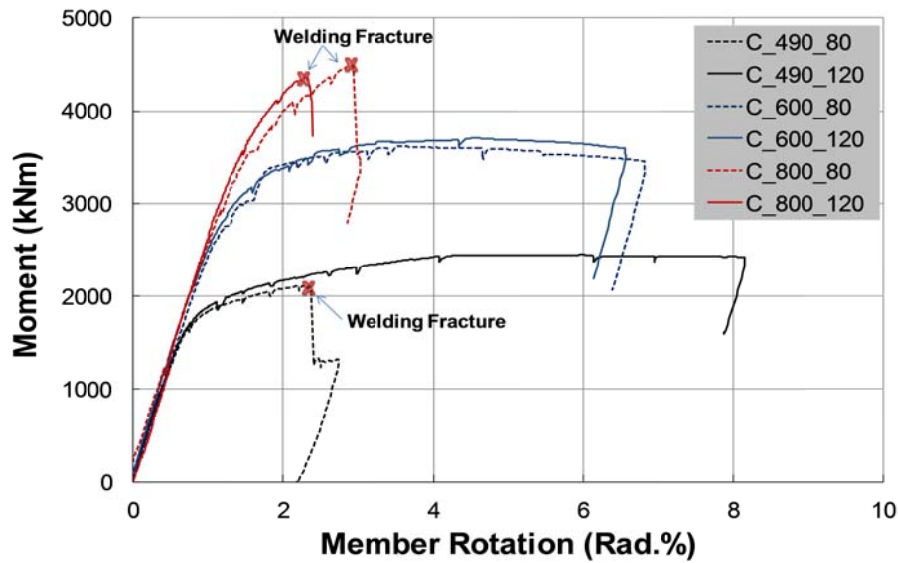


Fig. 8 Moment-rotation curves

Table 5 Initial stiffness

Specimen	Parameter		
	AISC-LRFD (kNm, × 100)	Test result (kNm, × 100)	Test result/theory
C_490_80	3350	2817.5	0.84
C_490_120	3535	2923.7	0.83
C_600_80	3350	2627.7	0.78
C_600_120	3535	3036.6	0.86
C_800_80	3350	2673.3	0.80
C_800_120	3535	3191.0	0.90

The predicted results from Eqs. (3)~(6) are compared with the current experimental results in Table 5. Results in this table clearly show that for CFTs with high-strength material, Eq. (3) gives the initial section stiffness about 10~22% higher than those of the tests. The AISC expression overestimates the stiffness for flexural tests. This is because the flexural CFT members have relatively little high-strength concrete in compression.

2.3.4 Ultimate load-carrying capacity

The ultimate load-carrying capacity is defined as the peak moment in test. Table 6 shows the maximum moments and rotation at the maximum moments of the specimens. The maximum moments obtained from the failure mode of local buckling were evaluated for this study since weld fracture was an undesirable and unpredictable failure.

For HSB600, the maximum moment of the specimen whose concrete compressive strength was

Table 6 Comparison of results

Specimen	Test results		AISC-LRFD (kNm)	Analysis Results (kNm)			
	Max. moment (kNm)	Rotation at max. moment (rad.%)		ALT1	ALT2	ALT3	ALT4
C_490_80	2114*	2.25*	1593	1852	1877	1844	1844
C_490_120	2445	6.00	1631	2342	2353	2281	2240
C_600_80	3617	3.57	2672	3231	3235	3157	3157
C_600_120	3706	4.53	2737	3254	3317	3167	3167
C_800_80	4497*	2.92*	4210	4488	4549	4496	4493
C_800_120	4362*	2.33*	4300	4571	4631	4527	4526

Note 1) *: Moment at Weld Fracture

Note 2) AISC2005: Use test data for Material Properties

Note 3) ALT1 (Nakahara), ALT2 (Steel Tube: Chung + Concrete: Liang), ALT3 (Liu), ALT4 (Steel Tube: Nakahara + Concrete: Liu)

120 MPa was slightly higher by 2% than that of the specimen whose concrete compressive strength was 80 MPa, as shown in Fig. 8. This is because high-strength concrete has negligible contribution to the strength of flexural composite members.

The comparison of SM490 and HSB600 steel with concrete compressive strength of 120 MPa showed that the maximum moment of the C_600_120 specimen was higher by at least about 52% than that of the C_490_120 specimen. Moreover, the rotation corresponding to the maximum moment on the C_490_120 specimen was higher by at least about 25% than that of the C_160_120 specimen. This is because the lower the strength of the steel tube is, the larger the strain at the local buckling occurrence on the steel tube. This indicates an identical tendency as the result of the local-buckling test on the square steel tube performed by Yamada *et al.* (1993).

The ultimate load-carrying capacity is calculated by AISC-LRFD code provision (Leon and Hajjar 2008) as follows

$$\begin{aligned}
 M_B &= Z_s F_y + 0.5 Z_c (0.85 f_{ck}) - Z_{sn} F_y - 0.5 Z_{cn} (0.85 f_{ck}) \\
 Z_c &= 0.25 h_1^3 \\
 Z_{sn} &= 2 t h_n^2 \\
 Z_{cn} &= h_1 h_n^2 \\
 h_n &= \frac{0.85 f_{ck} A_c}{2 [0.85 f_{ck} h_1 + 4 t F_y]} \leq \frac{h_1}{2} \\
 h_1 &= b - 2t
 \end{aligned} \tag{7}$$

where, b : width of steel tube
 t : thickness of steel tube
 A_c : area of inner concrete
 Z_s : full plastic section modulus of steel tube
 f_y : yield strength of steel tube
 f_{ck} : compressive strength of concrete

AISC was used the plastic stress distribution methods for predicting the resistance of CFT members subjected to bending and axial load. Here, f_y is the yield strength of steel tube and f_{ck} is the compressive strength of concrete. While the current code provision was not developed for high-strength CFT beam-columns, the experiment value also exceeded by more than 26%, compared to AISC-LRFD provision as shown in Table 6. The experimental data are employed to calibrate the design code.

2.3.5 Strain distribution in section

In each of Fig. 9, for the 6 specimens the distribution of strain across the depth of the section is shown for four different levels of moment. The measured strains vary considerably from the best fit straight lines. In C_490_120 specimen, top strains vary from about 626 to 5,673 μm . Bottom strains are very large varying from 910 about to 13,671 μm . The larger bottom strains occur, of course, because more of the steel must be in tension to balance the compressive force in the concrete. However, In C_600_80 specimen, top strains vary from about 848 to 14,685 μm . Bottom strains are slightly large varying from 918 about to 15,491 μm . For top and bottom flanges respectively, the maximum strains reached are about the same in tension and compression. This is

because the effect of concrete in steel tube is smaller than that for C_490_120 specimen.

For very small moments the positions of the neutral axis is unchanged, but soon cracking of the concrete occurs and the position shifts gradual upward about 5 to 15 mm. On the other hand, the positions of neutral axis for specimens using SM490 the position shifts gradual upward about 50 to 70 mm as the moment increases. This is because the effect of concrete in steel tube using SM490 is larger than those using HSB600 and HSA800.

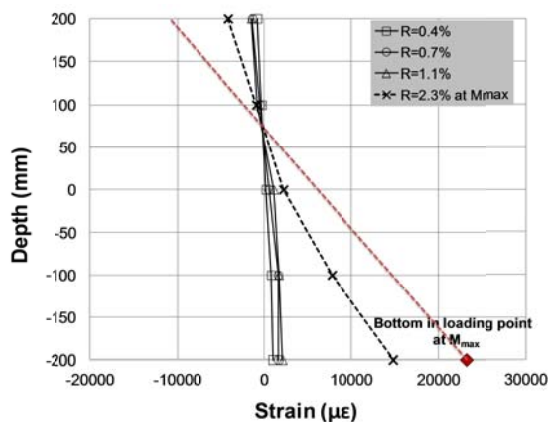
3. Numerical analysis of high-strength CFT members

3.1 Analytical method

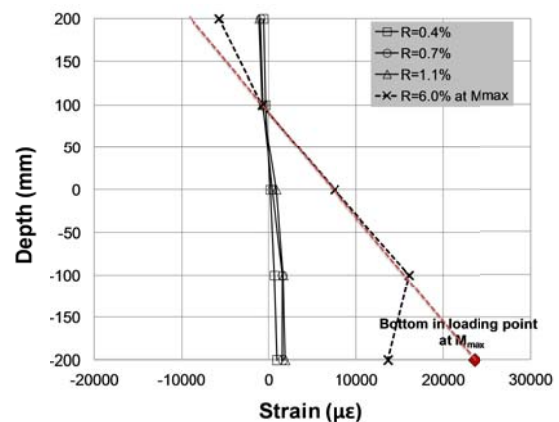
To estimate the structural behavior of high-strength CFT members under a cyclic bending moment, fiber element analysis was conducted based on numerical. Solution convergences are checked separately for both cross-section and member analyses.

The simplified nonlinear fiber element method is based on the following assumptions:

- (1) Assumed that Plane sections remain plane, and that there is no slip between the steel tube and concrete (Hajjar *et al.* 1998).
- (2) The stress-strain relation between the steel tube and the concrete at each point in the section follows the material model described in Section 3.2.
- (3) The material fibers in the cross-section are subjected only to uni-axial stress states.
- (4) The residual stress on the section is disregarded.
- (5) The tensile stress on the concrete is disregarded because the flexural behavior of square CFT section does not play an important role in tensile strength (Zang and Shahrooz 1997).
- (6) The wavelength of plastic local buckling from the loading point along the beam length is employed 0.8 times the width of the steel tube, based on flexural test results.
- (7) Elastic shear deformation is employed.



(a) C_490_80



(b) C_490_120

Fig. 9 Continued

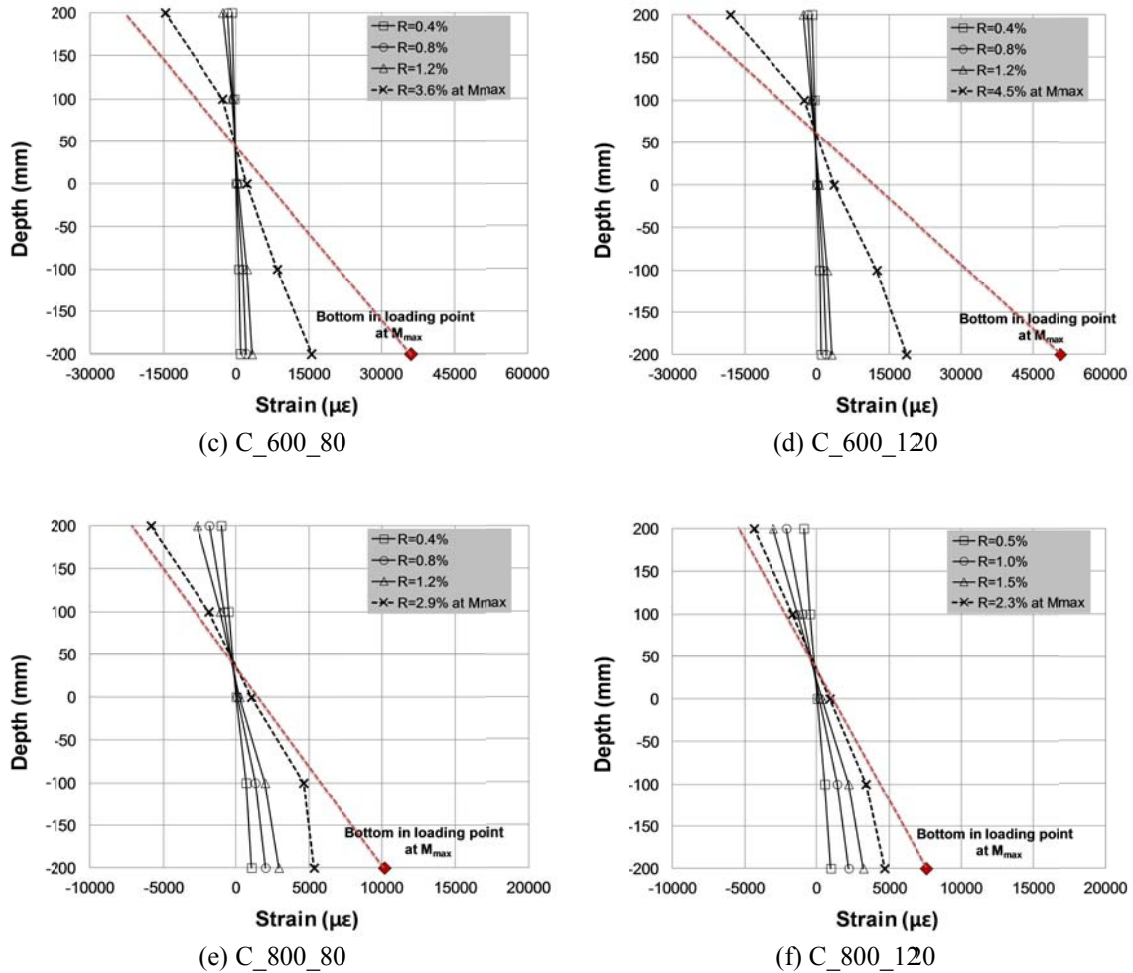


Fig. 9 Strain distribution across depth

For numerical analysis, the composite section is sub-divided into steel tube and concrete parts, and each of the steel tube and concrete sections is layered, as shown in Fig. 10(a). As shown in Fig. 10(b), the member near the loading point was divided longitudinally into 20 segments, each of which was 1/20 of the width of the steel tube. The rest was divided into 40 segments.

The sequence of the fiber element analysis is as follows:

- (1) Assumed a curvature in stage n and calculate the moment based on the force equilibrium in cross-section.
- (2) Under the moment-curvature ($M-\Phi$), the deflection of the member is calculated based on the concept that the curvature was integrated in the longitudinal direction.
- (3) The analysis was repeated under targeted flexural deflection.

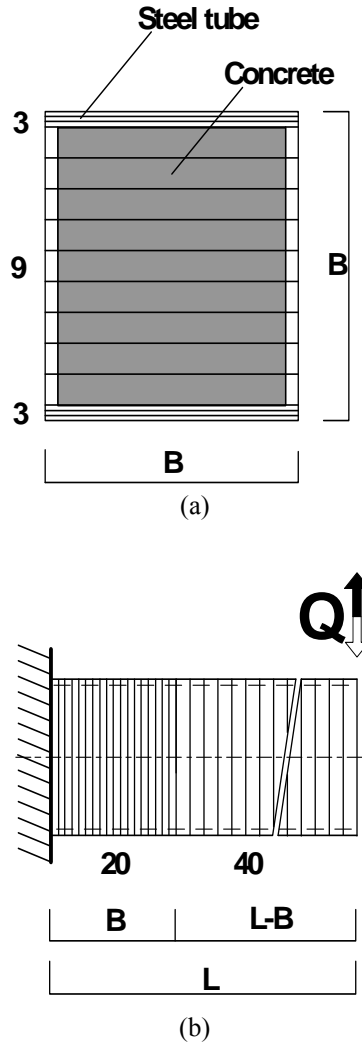


Fig. 10 Section and axial division: (a) sectional division; and (b) axial division

3.2 Stress-strain modeling

3.2.1 Steel tube

The tensile stress-strain relation shown in Fig. 3 was modeled by the material tensile test, and the stress-strain relation on the compressive side was modeled using different models proposed by past researchers for the local buckling of the square CFT member under compressive load:

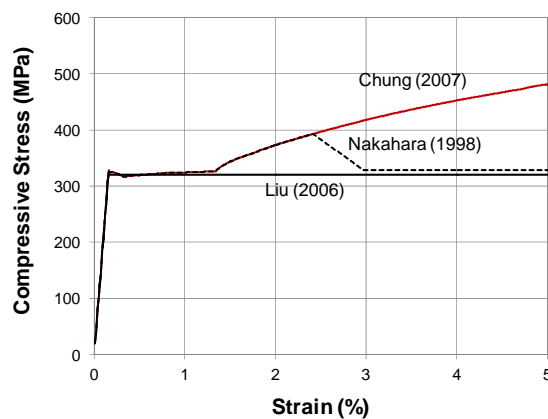
- (1) Chung *et al.* (2007) proposed a local buckling model for a steel tube considering the effect of the concrete on the CFT member based on a local buckling model of a steel tube under compression proposed by Yamada *et al.* (1993).

(2) Nakahara *et al.* (1998) proposed a model consisting of three zones: first, the strength degradation due to buckling within the elastic limit; second, considering the deterioration after reaching the yielding; and third considering the strain hardening corresponding to the width-thickness ratio (B/t) of the steel tube under the compression.

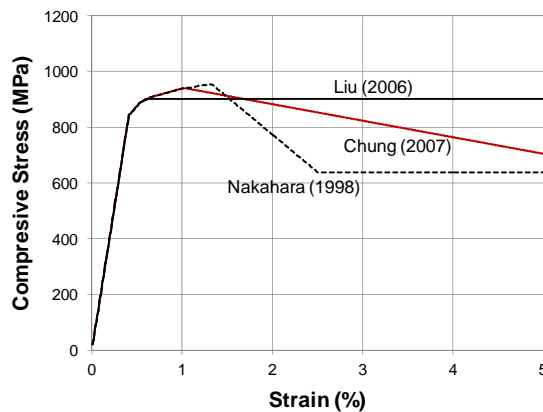
(3) Liu (2006) proposed an elastic-perfectly plastic model for steel tube.

The stress-strain relations on the compressive side obtained from the above three models, considering the strength and the width-thickness ratio of steel tube for specimen, are shown in Fig. 11.

For conventional 490 MPa rolled steel plate/sheet (SM490) for construction, the local buckling models proposed by Nakahara (1998) and Liu (2006) showed the stress-strain curve to be almost identical as compared with the model of Chung (2007). For HSA800 steel, the models proposed by Nakahara (1998) and Chung (2007) were more similar to each other than to the model proposed by



(a) SM490



(b) HSA800

Fig. 11 Stress-strain relationships in compression for steel tubes

Liu (2006). Meanwhile, when high-strength steel was used under the same width-thickness ratio, the models of Nakahara (1998) and Chung (2007) indicate that local buckling occurs early.

3.2.2 Concrete

The stress-strain relation used to model the concrete of the square CFT members considered the confinement effect of the steel tube and the strength of concrete proposed by past researchers:

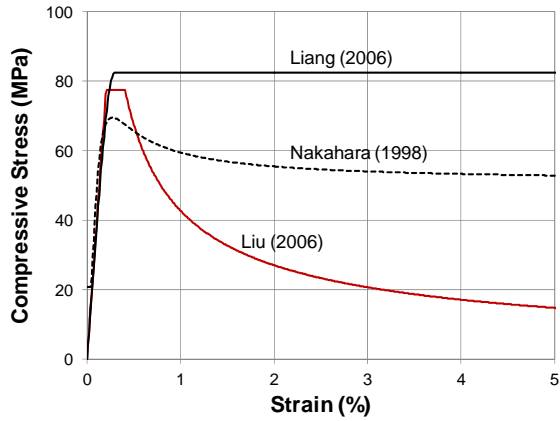
- (1) Nakahara *et al.* (1998) proposed a model in which the compressive strain simply increased at the maximum compressive stress without increasing the concrete strength for the confinement effect of the square CFT member. The stress-strain relation is expressed as a parabola, which consists of the nonlinear-increasing zone and nonlinear-decreasing zone after reaching maximum stress. The scale effect in the compressive strength of concrete reflected the equation obtained from the test results conducted by Blank and McNamara (1935). It was assumed that the steel tube would have no confinement effect on concrete because in elastic, the Poisson's ratio of concrete is smaller than that of the steel tube.
- (2) Liu's (2006) model consists of three zones: the rising zone, the maximum compressive stress zone, and the falling zone. The rising zone is the linear zone where the elastic modulus is multiplied by strain. The maximum compressive stress zone reflects the confinement effect of the steel tube to express the increase in maximum compressive strength and strain. The falling zone is nonlinear. The model considered no confinement effect of the steel tube on concrete in the rising zone.
- (3) Liang *et al.* (2006, 2009) also divided their model into three zones: the rising zone, which is the nonlinear zone proposed by Mander *et al.* (1988); the maximum compressive-stress zone, which reflects the increase in the strain due to the confinement effect of the steel tube; and the linear falling zone.

The stress-strain relation using the above three models and taking into account the confinement effect of the steel tube and the strength of concrete is shown in Fig. 12. Compared to the other models, Liang's (2006) model shows a very similar pattern regardless of the strength of steel tube and concrete because the width-thickness ratio of the steel tube was 20, which is small. Compared to the other models, Liu's (2006) model produced conservative results for concrete strength variation when the strain ratio was large due to the confinement effect. Liu (2006) also showed that the confinement effect increased when steel strength increased from SM490 to HSA800. Such a tendency clearly manifests when the compressive strength of concrete is at 80 MPa rather than at 120 MPa. The scale effect considered by Nakahara (1998) becomes larger as the strength of the materials becomes lower. The proposed model, which considered such a tendency, showed the lowest maximum stress compared to the other models.

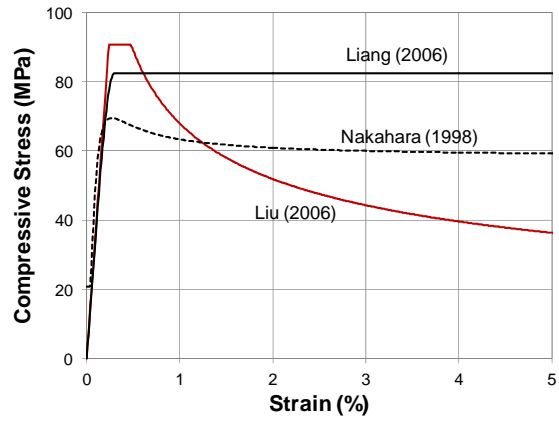
3.3 Comparison of the analytical and test results

Fig. 13 and Table 3 show the results of the comparison of the analytical results described in 3.1 and the test results. In addition, the effective initial stiffness and load-capacity using AISC-LRFD current code was shown in elastic-perfect plastic model.

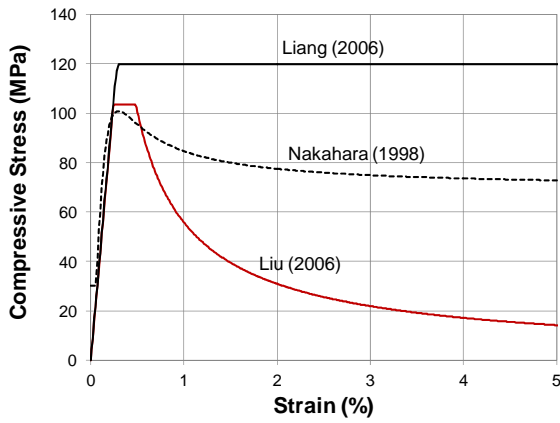
For the SM490 and HSB600 steel, the test and analysis results of the initial stiffness were almost identical regardless of the strength of the steel tube or concrete. For the rotation after



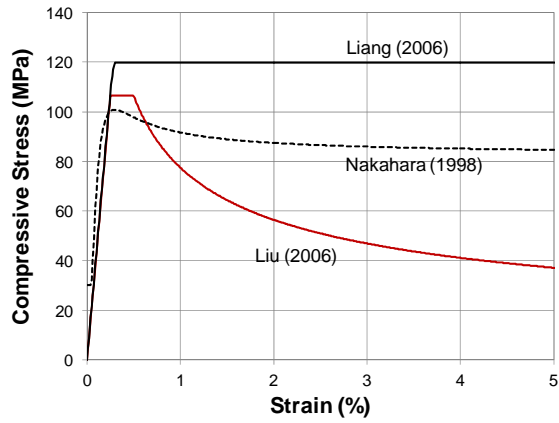
(a) Concrete: $f_{ck} = 82.5$ and steel: SM490



(b) Concrete: $f_{ck} = 82.5$ and steel: HSA800

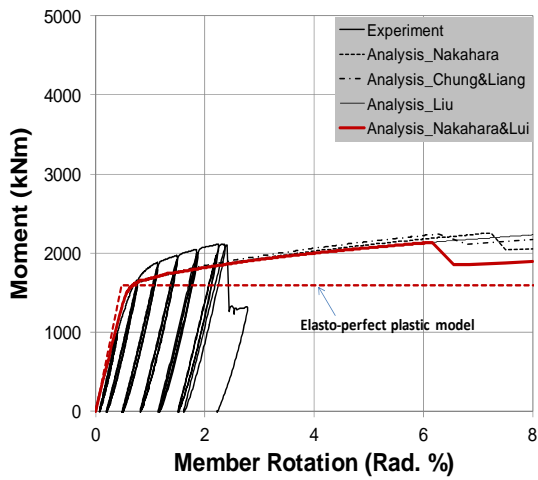


(c) Concrete: $f_{ck} = 119.7$ and steel: SM490

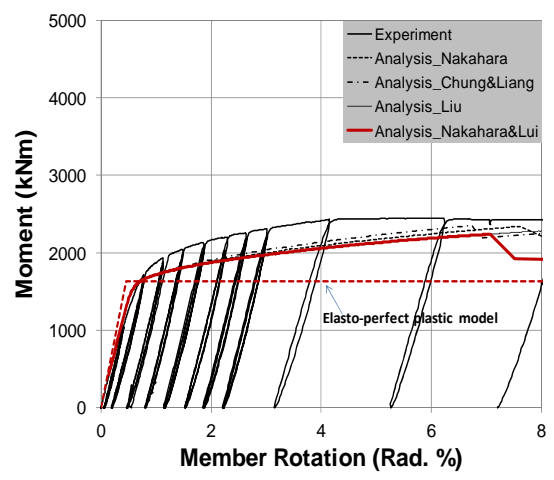


(d) Concrete: $f_{ck} = 119.7$ and steel: HSA800

Fig. 12 Comparison of stress-strain relationships for concrete



(a) C-490-80



(b) C-490-120

Fig. 13 Continued

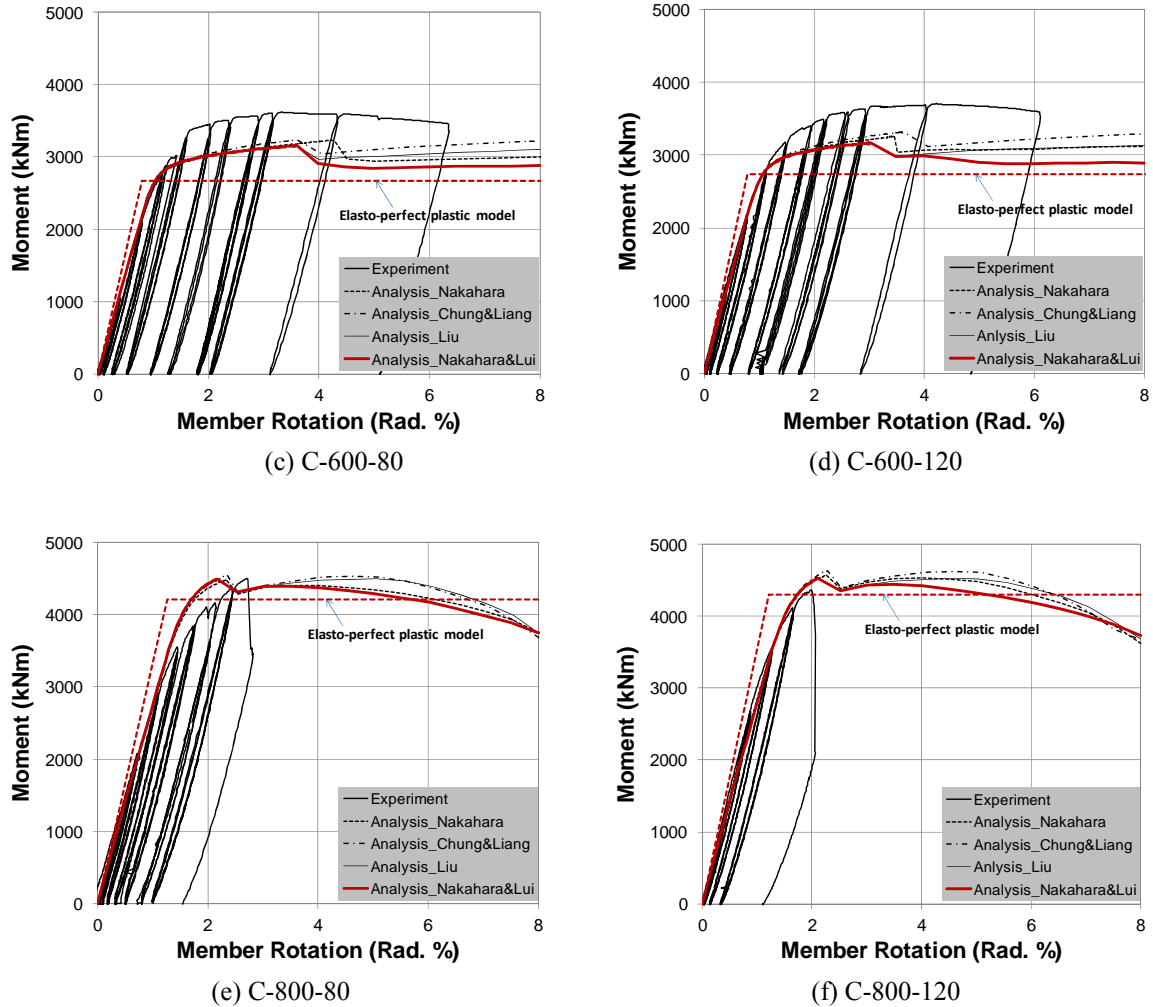


Fig. 13 Comparison of analytical and experimental results

yielding, the analysis value was about -6~15% of the test value at the maximum moment. For the HSA800 steel, the numerical analysis using the material model proposed by past researchers on the initial stiffness and yielding moment revealed almost identical results to that of the test.

The numerical analysis based on the material model proposed by the past researchers showed a minimal difference from the result of the test in terms of the initial stiffness and moment. This is because the influence of concrete strength in flexural behavior of high-strength CFT members was negligible. Fig. 6 shows strain distributions across the depth of the steel tubes at maximum moment. The maximum compressive strains reached are relatively small, approximately 5,000~30,000 μm .

And then, before the compressive stress-strain curves of the steel using different models are significantly different, the tests are reached up peak moment. On the other hand, ALT4 (Steel =

Nakahara's model and concrete = Liu's model) clearly exhibited strength degradation due to the local buckling.

4. Conclusions

This paper mainly deals with the static behaviour of square CFT members with high-strength materials. Based on the investigations above, it can be concluded that the structural behaviour can be conservatively predicted from the design provisions in the current AISC-LRFD code, the details is as shown following. Also, the fiber element analyses were conducted based on the material model considering the cyclic bending behavior of high-strength CFT members, which used high-strength steel tubes (SM490, HSB600, and HSA800, which is under development) and high-strength concrete ($f_{ck} = 80\sim 120$ MPa). The results obtained from comparing the numerical analyses and test results are as follows:

- (1) The failure mode for specimens was the local buckling on the flange at a distance that is half the width of the steel tube away from the loading points. This failure mode is also the common failure mode for normal-strength CFT members. However, specimens for HSA800 steel tubes were welding fracture of connection between endplate and steel tube. Further research is currently being conducted on welding method for high strength steel.
- (2) Test results showed that the difference in the initial stiffness was negligible regardless of strength of steel and concrete. Comparisons are made with the flexural stiffness using the existing AISC-LRFD codes for square CFT members. The equation (3) gives the initial section stiffness about 10~22% higher than that of the tests.
- (3) The standard is conservative in their prediction of the maximum load-carrying capacity regardless of high strength material. That is, the current AISC-LRFD design formula was verified, and proved to be reasonable and could be used in practice.
- (4) There was almost no difference in initial stiffness and moment for fiber element analytical results obtained from material model proposed by past researchers (Nakahara (1998), Chung (2007), Liang (2006), Liu (2006), etc.). Among the material models proposed by past researchers, the results obtained from the proposed models by Nakahara (1998) and Liu (2006), steel tube model proposed by Nakahara and concrete model proposed by Liu, were the most similar to the experimental results.
- (5) Comparison of the experimental and analytical results showed that the analysis value corresponding to the rotation of the maximum moment was estimated at about -6~15% of the test value. The initial stiffness from the analytical result was almost identical to the test result.

Acknowledgements

This research is supported by a grant from High-Tech Urban Development Program (09CHUD-A052272-01) funded by the Ministry of land, transport and maritime affairs.

References

- Blanks, R.F., and McNamara, C.C. (1935), Mass concrete tests in large cylinders, *ACI*, 31, 280-303.
- Choi Y.H., Kim K.S. and Choi S.M. (2008), "Simplified P-M interaction curve for square steel tube filled with high-strength concrete". *Thin-Walled structures*, **46**,506-515.
- Chung K.S., Chung J.A. and Choi S.M. (2007), "Prediction of pre- and post-peak behavior of concrete-filled square steel tube columns under cyclic loads using fiber element method", *Thin-Walled structures*, **45**, 747-758.
- Fujimoto T., Mukai, A., Nishiyama, I. and Sakino, K. (2004), "Behavior of eccentrically loaded concrete-filled steel tubular columns", *J. of Struct. Eng.*, ASCE, **130**, 203-212.
- Han L.H., Yang Y.F. and Tao Z. (2003), "Concrete-filled thin-walled steel SHS and RHS beam-columns subjected to cyclic loading", *Thin-Walled structures*, **41**(9), 801-833.
- Hajjar J.F., Molodan A. and Schiller P.H. (1998), "A distributed plasticity model for cyclic analysis of concrete-filled steel tube beam-columns and composite frames", *Eng. Struct.*, **20**(4-6), 398-412
- Hajjar, J.F., Schiller, P.H. and Molodan, A.A. (1998), "A distributed plasticity model for concrete-filled steel tube beam-columns with interlayer slip", *Eng. Struct.*, **20**(8), 663-676
- Leon R.F. and Hajjar J.F. (2008), "Limit state response of composite columns and beam-columns Part II: application of design provisions for the 2005 AISC specification", *Eng. J.*, 21-46.
- Liang Q.Q. (2009), "Strength and ductility of high strength concrete-filled steel tubular beam-columns", *J. of Constr. Steel Res.*, **65**(3),687-698.
- Liang Q.Q., Uy B. and Liew R. (2006), "Nonlinear analysis of concrete-filled thin-walled steel box columns with local buckling effects", *J. of Constr. Steel Res.*, 62(6), 581-591.
- Liu D. (2006), "Behavior of eccentrically loaded high-strength rectangular concrete-filled steel tubular columns", *J. of Constr. Steel Res.*, **62**(8),839-846.
- Liu D. and Gho W.M. (2005), "Axial load behavior of high-strength rectangular concrete-filled steel tubular stub columns", *Thin-Walled struct.*, **43**(8),1131-1142.
- Liu D., Gho W.M. and Yuan J. (2003), "Ultimate capacity of high-strength rectangular concrete-filled steel hollow section stub columns", *J. of Constr. Steel Res.*, **59**(12), 1499-1515.
- Mander JB, Priestley MJN, and Park R. (1988), "Theoretical stress-strain model for confined concrete", *J. of Struct. Eng.*, ASCE, **114**(8), 1807-26.
- Nakahara H., Sakino K., and Inai E. (1998), "Analytical model for axial compressive behavior of concrete filled square steel tubular columns", *Transaction of the Japan Concrete Institute*, **20**, 171-178 (In Japanese)
- Uy B. (2001a), "Strength of short concrete filled high strength steel box columns", *J. of Constr. Steel Res.*, **57**(2), 113-134.
- Uy B. (2001b), "Axial compressive strength of short steel and composite columns fabricated with high strength steel plate", *Steel. Compos. Struct.*, **1**(2), 171-185.
- Mursi M. and Uy B. (2004), "Strength of slender concrete filled high strength steel box columns", *J. of Constr. Steel Res.*, **60**(12), 1825-1848.
- Mursi M. and Uy B. (2006a), "Behavior and design of fabricated high strength steel columns subjected to biaxial bending. Part 1: Experiments, International Journal of Advanced Steel Construction", *Hong Kong Institute of Steel Construction*, **2**(4), 286-315.
- Mursi M. and Uy B. (2006b), "Behavior and design of fabricated high strength steel columns subjected to biaxial bending. Part 2: Analysis and design codes, International Journal of Advanced Steel Construction", *Hong Kong Institute of Steel Construction*, **2**(4), 316-354.
- Varma A.H., Ricles J.M., Sause R. and Lu L.W. (2002), "Experimental behavior of high strength square concrete-filled steel tube beam-columns", *J. of Struct. Eng. ASCE*, **128**(3), 309-318.
- Varma A.H., Ricles J.M., Sause R. and Lu L.W. (2004), "Seismic behavior and design of high-strength square concrete-filled steel tube beam columns", *J. of Struct. Eng. ASCE*, **130**(2), 169-179.
- Yamada S., Akiyama H. and Kuwamura H. (1993), "Post-buckling and deteriorating behavior of box-section

steel members”, *J. of Struct. Constr. Eng.* AIJ 444,135-143. (In Japanese)
Zhang W. and Shahrooz B.M. (1997), “Analytical and experimental studies into behavior of concrete-filled tubular columns”, Report no. UC-CII 97/01, College of Engineering, Cincinnati Infrastructure Institute, University of Cincinnati, OH.

UY